Energy confinement and thermal boundary conductance effects on short-pulsed thermal ablation thresholds in thin films

John A. Tomko, Ashutosh Giri, Brian F. Donovan, Daniel M. Bubb, Sean M. O'Malley, and Patrick E. Hopkins

Phys. Rev. B **96**, 014108 — Published 12 July 2017

DOI: 10.1103/PhysRevB.96.014108

Energy confinement and thermal boundary conductance effects on short-pulsed thermal ablation thresholds in thin films

John A. Tomko,[1] Ashutosh Giri,[2] Brian F. Donovan,[3] Daniel M. Bubb,[4] Sean M. O'Malley,[4] and Patrick E. Hopkins[2,*]

[1]*Department of Materials Science and Engineering, University of Virginia, Charlottesville, VA 22904, USA*
[2]*Department of Mechanical and Aerospace Engineering, University of Virginia, Charlottesville, VA 22904, USA*
[3]*Department of Physics, United States Naval Academy, Annapolis, MD, 21402, USA*
[4]*Department of Physics, Rutgers University - Camden, 227 Penn Street, Camden, N.J. 08102*

(Dated: June 16, 2017)

For this work, single-pulse ablation mechanisms of ultra-fast laser pulses (25 ps) were studied for thin gold films (65 nm) on an array of substrates with varying physical properties. Using time-domain thermoreflectance (TDTR), the interfacial properties of the thin film systems are measured; in particular, the thermal boundary conductance. We find that a often used, and widely accepted equation describing threshold fluences of homogeneous bulk targets breaks down at the nanoscale. Rather than relying solely on the properties of the ablated Au film, the ablation threshold of these Au/substrate systems is found to be dependent on the measured thermal boundary conductance; we additionally find no discernible trend between the damage threshold and properties of the underlying substrate. These results are discussed in terms of diffusive thermal transport and the interfacial bond strength.

I. INTRODUCTION

Ablation, from a thermodynamic standpoint, is the process of evaporative material removal when a critical temperature is reached. However, laser-induced ablation has become a general term referencing any laser-induced mass removal, with expected ejection mechanisms ranging from non-thermal, photomechanical spallation [1–3] to a thermally-driven vaporization process [4, 5]. This mixture of mechanisms and definitions has clouded the current understanding of the basic heat transport processes that drive material ablation [1, 3, 6], especially when considering thin films and nanocomposites. On the nanoscale, the high densities of inclusions, defects and interfaces can lead to thermal transport properties in materials that can be drastically varying from those intrinsic to their respective bulk phases [7, 8]. Thus, an understanding of the heat transport processes that drive material ablation in nanosystems is lacking; this lack of understanding is amplified by the aforementioned ambiguities in the role of diffusive thermal transport and thermal resistance in bulk materials during laser ablation.

Diffusive heat transport generally drives ablation processes in materials when the characteristic energy deposition time (i.e., pulse width, t_p) is much greater than the electron-phonon equilibration time (τ_{ep}) [1]. In this temporal regime, the electrons and lattice are in equilibrium during the majority of the laser pulse absorption; thus, the assumption of $T_e \sim T_i$ is valid, where T_e is the electron temperature and T_i is the ion temperature. In this "thermal ablation" regime [1], thermal expansion limits the ablation threshold, hence defining the condition that the absorbed laser energy must be fully converted into the energy of the broken bonds in some thickness defined by a thermal penetration depth of the pulse ($\delta_T = (\alpha t_p)^{1/2}$, where α is the thermal diffusivity). In this regime, the thermal ablation threshold, which determines the onset of the material removal process, follows the well known $\sqrt{t_p}$ pulse width dependence [2, 9], given by [1]

$$F_T \approx \frac{(\alpha t_p)^{1/2} \varepsilon_b n_a}{A}, \tag{1}$$

where ε_b is the atomic binding energy, n_a is the number density of atoms in the target, and A is the absorptivity of the material.

The threshold fluence given in Eq. 1 is derived by performing a basic energy balance with the absorbed laser pulse and the heat equation used to describe diffusive thermal transport in a homogeneous material [1]. This threshold applied to thin films and nanosystems is thus questionable, as previously mentioned, the heterogeneity induced from interfaces and inclusions can lead to thermal transport properties to be vastly different from that of the homogeneous bulk phase [7, 8]. For example, when film thickness approaches δ_T, interfaces and boundaries adjacent to these thin films can pose significant thermal resistance that impede heat flow out of locally heated volumes in thin films. Indeed, this finite thermal boundary conductance, h_K, can represent a limiting thermal resistance in a wide array of thin films and nanosystems [10–13]. Furthermore, for thermal ablation conditions (i.e., when $t_p >> \tau_{ep}$, as previously mentioned), thermal diffusion could be dominated by the thermal boundary conductance as opposed to the thermal properties of the film or substrate. For example, characteristic time scales associated with the interfacial temperature drop [14] driven by h_K are estimated as $\tau_{int} = Cd/h_K$, where C and d are the heat capacity and film thickness of the thin film material [15]. For a homogeneously heated Au film where $d \approx 100$ nm (the ballistic penetration depth of electrons after laser irradiation in Au is $\sim$100 nm) [16], the time scale necessary for complete diffusion of energy across an Au film on a substrate is $\sim$5 ns, assuming h_K is $\sim$50 MW m^{-2} K^{-1} [17–19]. Thus in the regime where this timescale is two orders of magnitude greater than laser deposition time (e.g., when using picosecond pulses), the thermal energy deposited by the laser

pulse would be intially confined in the volume of the film. As thermal ablation processes occur up to nanosecond timescales [20] and are greatly affected by the ablated material's temperature [6], energy diffusion, limited by the interfacial thermal resistance, would be expected to play a role in such processes in thin films.

To the best of our knowledge, this effect of thermal confinement during thermal ablation conditions has never been experimentally and systematically investigated, leaving a large void in the understanding of how Eq. 1 applies to thin film systems for predicting ablation thresholds. Qualitatively, in this temporal regime where the deposited laser energy is confined in the thin films due to a thermal boundary resistance at the film/substrate interface, it would be expected that lower applied fluences would be necessary for ablation to occur, as less energy from the absorbed laser pulse is necessary for equivalent power densities in a thin films compared to its bulk counterpart. Thus, in this regime with increasing interface conductances, thermal energy is better coupled to the substrate, and the ablation threshold should correspondingly increase.

An additional consideration in applying Eq. 1 to thin films lies in the binding energy terms, ε_b, as the interatomic cohesion forces of a pure material are not the only forces present in the thin film on substrate system. This is evident throughout literature [21–23] for laser ablation in liquids; the overlying liquid layer mechanically confines the system and becomes an additional force that the spalled material must overcome, thus leading to an increase in the relative ablation threshold for that material. In this context, for thin films, the binding energy term must also be related to the interfacial bonding environment between the film and the substrate as the film must overcome the work of adhesion at this interface. Note, this interfacial bond strength can be intimately related to the thermal boundary conductance across solid/solid interfaces [10, 24–29].

This work seeks to elucidate the role of diffusive thermal transport mechanisms during short-pulse laser ablation of thin films. When the film thickness approaches the length and time scales associated with energy diffusion, thermal boundary resistances are expected to influence the ablation threshold of a material. In this work, we experimentally demonstrate the failure of Eq. 1 for predicting the ablation threshold for thin films. By obtaining the ablation threshold of gold thin films deposited on various substrates with varying thermal boundary conductances across the Au/substrate interfaces, we find that the thermal confinement within the film controls both the damage threshold and the heat-affected zone.

II. METHODS

II.A Sample fabrication

We conducted the thermal ablation threshold and thermal boundary conductance measurements on 65 nm Au films on different substrates with varying interfacial resistances. The Au films were electron-beam deposited on fused silica (SiO_2), silicon, nickel, titanium, sapphire (Al_2O_3, and copper substrates; all substrates were purchased from MTI corporation. Prior to deposition, the substrates are rinsed with acetone, ethanol, and methanol then subsequently dried with nitrogen gas. Note, no efforts to remove native oxides on certain substrates were undertaken.

II.B. Picosecond laser ablation

The single-pulse ablation threshold experiments utilized a 25 picosecond Nd:YAG laser operating at its fundamental wavelength of 1064 nm as shown in Fig. 1a. The beam size is experimentally determined with the knife-edge method for both air and liquid environments. We also use the beam waist, ω_0, as a fitting parameter during threshold measurements for confirmation of the spot size at the target surface; the two methods are in good agreement for bulk targets. In the case of our thin films, as discussed in detail later, we find that the best-fit value for the beam-waist increases with increasing thermal boundary conductance. This phenomenon is attributed to in-plane thermal diffusion during the ablation process. The thermal ablation threshold for these 25 picosecond pulses is determined in each Au/substrate system by measuring the induced damage area as a function of incident laser fluence. The results are then fit to [30]

$$D^2 = 2\omega_0^2 ln(\frac{F}{F_{\text{th}}}) \tag{2}$$

where both ω_0, the beam waist, and F_{th}, the ablation threshold are used as free parameters to the best-fit, while D is the diameter of the ablation area and F is the applied fluence and are experimentally measured. The ablation measurements were performed in both air and water environments; in the liquid environment, the target was submerged in 15 mm of pure DDI water utilizing a flow cell, as described in [22, 31], to avoid scattering with pre-existing nanoparticles. The subsequent damage area was measured using dark-field optical microscopy which matches the damage areas measured via scanning electron microscopy. This method of measuring damage areas has been shown to provide similar and accurate results to other methods of determining damage and ablation thresholds [32]. It should be noted that our ablation 'crater' depth is limited to the thickness of our films and there is no visible damage to the substrates in values used for the threshold measurements; we emphasize the lack of *visible* damage to the substrate in our measurements, as there may be underlying microstructure alteration and formation of defects not observable in our microscopy characterization. Further, we find redeposition of ablated material on the substrate surface, indicitive of droplet formation. This finding implies that at least one mechanism leading to thermal ablation in this work is phase explosion; the possibility of this phase-transformation occurring simultaneous to other ejection processes is discussed later.

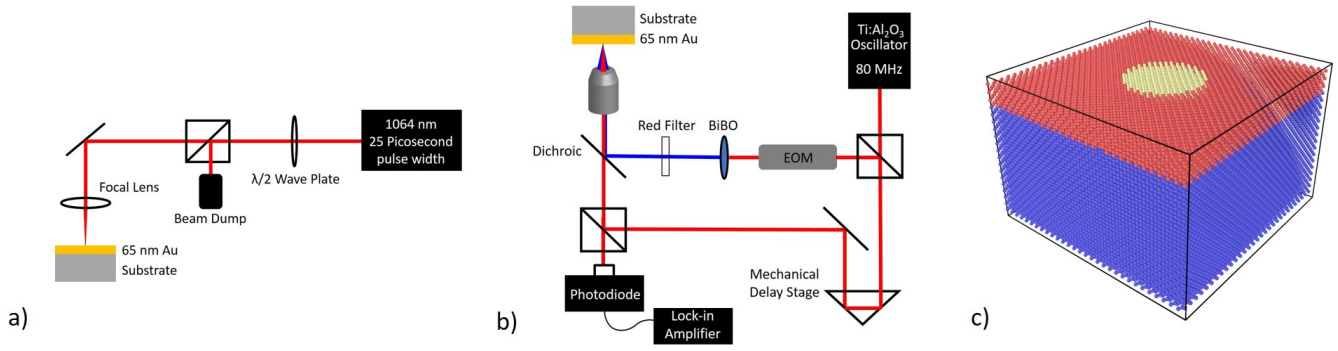

Figure 1. a) A schematic of the experimental set-up for the ablation threshold experiments. The Au/substrate sample is placed in a liquid cell for threshold measurements in water. b) A schematic of the experimental set-up for our TDTR measurements. c) A schematic of the computational domain representing a thin film (red and yellow atoms) on a substrate (blue atoms) described by the Lennard-Jones potential.

III.C. Time-domain thermoreflectance

For measurement of the interfacial thermal resistance, we utilize a two-color TDTR scheme, as described in more detail elsewhere [33–35] and graphically depicted in Fig. 1b.Our TDTR system is centered around a Spectra Physics Tsunami Ti:Sapphire oscillator, emanating ∼90 fs, 800 nm (center wavelength with 10.5 nm bandwidth) pulses at an 80 MHz repetition rate. The output of the oscillator is split into pump and probe paths. The pump, after passing through an electro-optical modulator and a second-harmonic generation crystal, is converted to a modulated pulse train of 400 nm pulses; in this work, we modulate the pump train at 8.8 MHz. The probe pulses are mechanically delayed to known time intervals relative to the pump pulse. We monitor the in-phase and out-of-phase voltages from the reflected probe pulses at the frequency of the pump modulation frequency with a lock-in-amplifier. These lock-in signals are related to the surface temperature of the Au film, and are related to the thermal properties of the samples, including the Au/substrate thermal boundary conductance [15, 36–38]. The in-phase data is fit to a thermal model where the thermal boundary conductance is our free parameter [33, 39, 40]; the thermal conductivity of the film and substrate are obtained from literature values [41–43] and the film thicknesses are determined from profilometry measurements. The measured thermal boundary conductance and associated error is obtained from measuring five spots on the film.

II.D. Molecular dynamics simulations

To explore the nanoscopic mechanisms responsible for dictating thin film damage, we perform molecular dynamics (MD) simulations on representative thin films with varying boundary conditions with the region defined by substrate atoms. For our MD simulations, we employ the widely used 6-12 Lennard Jones (LJ) potential, $U(r) = 4\varepsilon[(\sigma/r)^{12} - (\sigma/r)^6]$, where U is the interatomic potential, r is the interatomic separation, and σ and ε are the LJ length and energy parameters, respectively. The cutoff distance is set to 2.5σ (for computational efficiency) with the time step for all simulations set to 0.1 fs. As we are interested in understanding the effects of TBC on the damage area in thin films in general, the use of LJ potential is sufficient to provide qualitative insight. For the thin films, the length and energy parameters are modeled for argon with σ_s=3.405 $\AA$ and ε_s=10.3 meV and the atoms are placed in an fcc structure with a lattice constant of a_0=1.56σ. The substrate atoms are also placed in an fcc lattice with the same lattice constant, and the energy and length parameters are set to σ_s=3.405 $\AA$ and ε_s=10.3 meV, respectively. To mimic a weakly bonded interface, the film-substrate energy parameter is set to ε_{f-s}=2.6 meV, whereas, for the strongly bonded interface, ε_{f-s}=10.3 meV. The sizes of the computational domains are $30a_0 \times 30a_0 \times 20a_0$ with periodic boundary conditions applied in all directions. The mass for all atoms is set to 40 g mol^{-1}.

Initially the computational domains are equilibrated under the Nose-Hoover thermostat [44], and the number of atoms, volume and temperature of the simulation are held constant followed by the NPT integration, which is the isothermal-isobaric ensemble with the number of particles, pressure and temperature of the system held constant for a total of 1.5 ns at 0 bar pressure and 70 K temperature. To melt a region of the thin film, we heat the atoms contained in a cylindrical area in the center of the thin film at a temperature of 300 K (under the NVT ensemble, with the number of particles, volume and temperature held constant) for a total of 1 ns after equilibration, while the NVT integration at a temperature of 70 K is simultaneously applied to the rest of the computational domain; note, the melting temperature of LJ argon is 87 K [45]. A schematic of the computational domain is shown in Fig. 1c, where the red atoms represent the thin film, the yellow atoms represent the melted region in the thin film and the blue atoms represent the substrate.

After we melt the cylindrical region in the thin film, the atoms in the thin film region are allowed to equilibrate under the NVE integration, which is the microcanonical ensemble

with the number of atoms, volume and the energy held constant, while the substrate atoms are simulated under the NVT integration. We monitor the melted regions of the computational domains with the varying boundary conditions between the film and the substrate atoms to shine more light on the influence of the different mechanisms that dictate diffusive damage of thin films. The results of these simulations are discussed in detail in the following section.

III. RESULTS AND DISCUSSION

Figure 2a shows the measured thermal ablation threshold values for the various Au films as a function of substrate thermal conductivity. The lack of substrate dependence suggests that the thermal properties of the substrate are not primary factors dictating the different ablation thresholds in the thin Au films; note, we find a similar lack-of-trend is found in the thermal ablation threshold as a function of substrate effusivity. Furthermore, even if a general monotonic decrease trend could be gleaned from Fig. 2a, these data would suggest that the faster in which heat is being transferred away from the heat-affected zone and into the bulk of the substrate heat sink, the lower the ablation threshold, which is counterintuitive from a simple energy balance argument. This suggests another energy diffusion mechanism must be limiting the ablation threshold in these films on substrate systems.

As we discussed previously, due to the typical times scales of thermal diffusion, we hypothesize that the thermal boundary conductance, h_K, at the Au/substrate interface imposes the limiting resistance that will dictate thermal ablation of the Au films under these conditions. We plot the thermal ablation threshold in ambient conditions as a function of measured h_K for the various Au/substrate interfaces in Fig. 2b. We find that the ablation threshold of these systems scales linearly with their respective thermal boundary conductances as shown in Fig. 2b, supporting our hypothesis that h_K at the film/substrate interface can influence the thermal ablation threshold more directly than the substrate thermal properties. The measured thermal boundary conductances agree well with previously reported values for various Au/substrate interfaces [17–19, 27, 35]. The thermal boundary conductance is a diffusive thermal resistance that is well known to impact the overall heat transport in thin films and nanosystems. Thus, our data suggest that thermal ablation thresholds in this picosecond regime are related to the heat transport mechanisms that underpin the diffusive thermal resistance at the film/substrate interface.

In the "bulk" limit of ablation thresholds, previous experimental [22] and computational [1] works have determined threshold values for bulk Au targets through numerous methods, with reasonable agreement at 0.210 J cm^{-2} and 0.245 J cm^{-2}, respectively, in ambient conditions; the experimental value was reported as slightly lower than theory due to a roughened surface, leading to an enhancement in photon absorption [22, 46]. Under these circumstances, Eq. 1 is valid as only the properties of a pure substance must be considered (in particular, a constant thermal diffusivity and cohesion energy can be assumed). Thus, in the limit where interfacial resistances are large and thus confine thermal energy to the volume of the thin film, the ablation threshold approaches the previously measured bulk damage threshold.

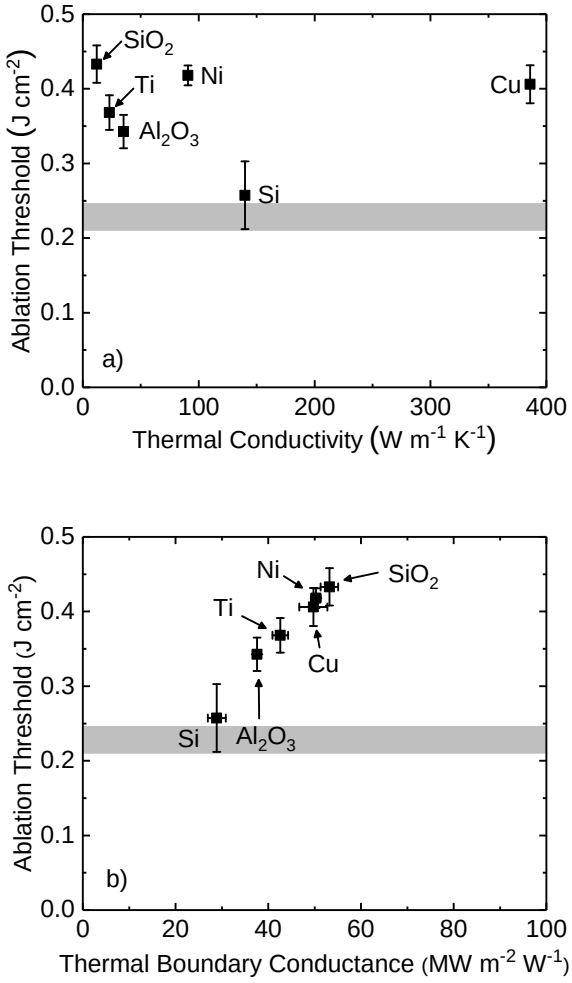

Figure 2. a) Measured ablation thresholds of Au films as a function of the associated substrate's thermal conductivity. b) The thermal ablation thresholds as a function of the measured thermal boundary conductance between Au films and the labeled substrates. The gray bar represents range of previously reported values for the 'bulk' ablation threshold of Au in air [1, 22].

The primary mechanisms driving laser ablation of thin films is typically discussed in terms of delamination and ejection of condensed material due to thermo-mechanical effects at the interface [47, 48]. Though, even in the case of laser-induced forward transfer (LIFT), previous experimental works using picosecond pulses have shown the process to follow melting dynamics in fashion similar to that of nanosecond melting of thin films [49]. Furthermore, as shown by numerous computational works, at higher fluences, phase explosion (or

an analogous phase-transformation such as explosive boiling, whereby the material is transformed into a metastable liquid state) occurs and is the primary mechanism for material ejection [23, 50, 51]; a mechanism occurring independent of the ablated materials thickness. As our threshold measurements are derived from a fit to Liu's equation over a large span of applied fluences, it is likely that a complex mix of these dynamics occurs within the heated volume simultaneously, potentially dependent on fluence. This is further supported by two observations of the damaged region: Redeposition of ablated material and delamination of the surrounding film. Droplet formation during ablation, a consequence of explosive boiling or phase explosion, is known to lead to redeposition of such droplets on the target surface, which we observe in our microscopy images. Furthermore, we find delamination outside the area in which material is ejected, indicating that a thermomechanical mechanism occurs simultaneous to phase explosion. Nonetheless, regardless of mechanism, as Eq. 1 is derived from a basic energy balance, the binding term, ε_b, references the energy necessary to overcome some adhesive force. Typically, this term implicitly references the binding energy between two atoms within a material (i.e., atomic disintegration). In a thin film system, the interfacial atoms have some adhesive force between the film and substrate, which can be overcome. During a gas-phase transformation, these interfacial atoms would play less of a role, making the binding energy a more negligible term, as the disintegration energy in the bulk of the film would be the dominant adhesive force to be overcome for the material's ablation threshold. This does not imply the interface is to be neglected; should heat be efficiently dissipated into the substrate, the Au film could rapidly drop below the temperature necessary for the phase-transformation, and remain adhered in condensed phase. On the contrary, should mechanical spallation be the primary ejection mechanism, one would expect the interfacial adhesion to be the dominating term, as it is the weakest energy to overcome, and the bulk of the film would spall once reached. As discussed later, the measured value of thermal boundary conductance is known to be related to both phonon mismatch at the interface as well as interfacial bonding. Thus, the TBC reflects both dissipation rate and adhesion of the film.

To study this hypothesis in more detail, we repeat the ablation threshold experiments on the same Au/substrate systems while submerged in 15 mm of DI water, as depicted by the open circles in Fig. 3. The thermal ablation thresholds are higher for the Au films when submerged in liquid as compared to the air experiments, but only for the Au/substrate systems with the highest h_K's; in other words, as the thermal boundary conductance is lowered (resistance is increased), the presence of the liquid on the Au has a reduced effect. In the limit of Au/Si (lowest h_K), the liquid layer does not affect the ablation threshold. This further supports our discussion regarding diffusive heat transport across the nanoscale interfaces as the underlying mechanisms affecting thermal ablation. The addition of the liquid layer, and resulting Au/water interface conductance, creates an additional parallel path for thermal transport out of the Au film. In Fig. 3, an additional thermal boundary conductance of 50 $\pm$ 30 MW m^{-2} K^{-1} is assumed for the Au/liquid interface [40, 52, 53]. As can be seen, the lower values for h_K (higher resistances at the Au/substrate interface), such as Au/Si, the additional thermal pathway is not large enough to drastically affect this threshold, and it does not deviate far from the theoretical minimum value found in previous literature [22]. Though the nominal value of ablation threshold for Au on Si substrates appears independent of environment, the large error associated with both the measured threshold and previous measurements of thermal boundary conductance at a solid/water interface leaves the possibility of it being within the linear range found in the solid/solid interfacial conductances. Additionally, although they can not be accounted for in error bars, phenomena leading to damage outside of thermal effects should be considered during ablation in a liquid environment. For example, cavitation and plasma confinement are hypothesized to lead to secondary erosion effects during laser ablation in liquids [22].

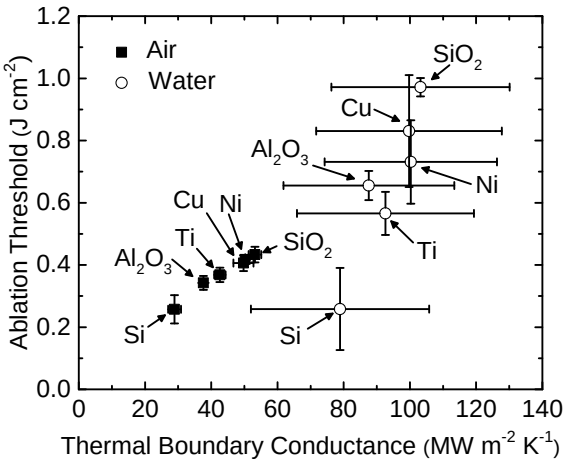

Figure 3. Ablation thresholds against the thermal boundary conductance in air (black squares) and liquid (open circles) environments, where the Au/liquid interface is assumed to have a thermal boundary conductance of 50 $\pm$ 30 MW m^{-2} K^{-1}; as the liquid provides a parallel path for thermal transport, the Au/water interfacial conductance can be summed with the measured Au/substrate interface.

Furthermore, given the relatively modest increase in pressure with the addition of water on the Au surface ($\sim$150 Pa), we do not believe this change in thermal ablation threshold upon liquid submersion is due to an increase in mechanical confinement from the additional pressure. While an increase in ablation threshold has been observed during laser ablation in liquids [22, 50] due to mechanical confinement of the spalled material, previous work by Losego *et al.* [27] has shown that pressures on the order of MPa are necessary for spallation to occur for 80 nm Au films. This suggests orders of magnitude more pressure from the liquid addition would be necessary to impact the thermal ablation threshold if the liquid

was mechanically confining the thermally excited Au.

As an additional experiment to support our assertion that the thermal boundary conductance at the Au/substrate interface is the limiting factor impacting thermal ablation thresholds, we considered the measured damage area of the Au films on the different substrates, as shown in Fig. 4. The damage area trends inversely to thermal boundary conductance (i.e., higher damage areas for the Au/substrate samples with lower h_K at a set fluence). In the time scale of the diffusive damage (i.e., nanoseconds [54]), competing thermal diffusion processes are occurring, namely, diffusion across the Au/substrate interface and in-plane thermal diffusion in the Au film. A reduction in thermal boundary conductance promotes increased in-plane diffusion of the deposited energy, which leads to an increase in damaged area. This hypothesis is further supported by the increasing best-fit value of the beam waist, ω_0, with increasing thermal boundary conductance as shown in Fig. 4. As Eq. 2 is derived for one-dimensional transport, a fitted value larger than the experimental beam-waist would be expected should lateral transport begin to play a substantial role in the ablation process. In the original derivation of Eq. 2, Liu found sound agreement between the measured area of a laser-induced amorphous region and the incident laser-energy profile, indicating negligible lateral thermal transport during picosecond-laser-induced phase transformations [30]. As we find the beam waist in his interpolation model to deviate from the experimentally-measured beam waist, which is held constant during the ablation experiments, this further supports our posit regarding a thermal boundary conductance-limiting thermal ablation threshold in these films. For example, at a set fluence, one would expect that a larger beam waist results in a lower *effective* fluence, thus decreasing the damage area at a constant incident power; this is equivalent to a constant beam waist with power dissipated from the thin film to a supporting substrate due to enhanced cross-plane thermal transport.

Given this, it is evident that Eq. 1 cannot accurately be applied to nanosystems and thin films without modification of various terms; the threshold is very clearly dependent on the thermal boundary conductance present at the film interface. Thus, we turn our discussion now to the underlying nanoscale heat transport mechanisms that are impacting thermal ablation of thin films, which will lead to the necessary understanding required for future studies to derive thin film equivalents of Eq. 1. Thermal transport across a thin film and its underlying substrate, and hence the measured h_K, can be influenced by numerous factors, which has been reviewed in detail in previous works [10, 12]. Most notably in relation to our thermal ablation data, we focus on the following three factors that can drive changes in thermal boundary conductance: i) lattice temperature, ii) phonon spectrum mismatch and iii) interfacial bonding.

i) Temperature: Assuming elastic phonon scattering at the Au/substrate interface [55–59], the phonon thermal boundary conductance from the Au film to the substrate will follow temperature trends similar to that of the lattice heat capacity of Au. In other words, the thermal boundary conductance will be relatively constant above the Debye temperature of Au ($\sim$165 K). Due to the relatively weak mechanical bond at the Au/substrate interface (especially given the fact that we make no effort to remove native oxides on some of the substrates) [18, 27, 35], we do not expect inelastic processes to dominate the measured h_K across these interfaces [26, 60]. Furthermore, on these thermal ablation time scales, we do not expect hot electron-interface or substrate coupling to play a role, as the time scale for this excited electron-phonon processes has been shown to only influence heat transport within a few picoseconds after laser heating [35, 61–63]. Along these lines, previous works have shown that after electron-phonon equilibration following pulse excitation, which takes place within a few picoseconds in Au, the thermal boundary conductance is dominated solely by phonon interaction between the film and substrate [35, 59, 64]. Thus, even though these thermal boundary conductance measurements have not been extended to the high-temperature regime representative of when thermal ablation occurs, it is unlikely the trend in h_K vs. substrate would shift. Therefore, we surmise that the trends in h_K shown in Fig. 2 to be representative of the phonon resistance mechanisms influencing thermal ablation. To understand the underlying phonon coupling that influences our measured thermal ablation thresholds, we now focus our discussion on the role of phonon spectrum mismatch and interfacial bonding effects.

ii) Phonon spectrum mismatch: To a decent first approximation, the phonon energy transmission across solid interfaces can be related to the spectral overlap of the phonon densities of states between the film and substrate [11, 17, 65]. This could indeed be the limiting factor in our thermal abla-

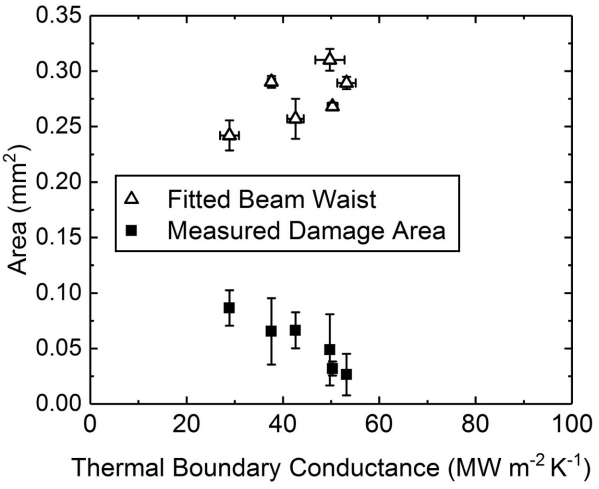

Figure 4. Observed damage areas of each Au/substrate system at a fluence of $\sim$0.94 J cm^{-2} and the beam-waist value obtained from fitting to Eq. 2. With increasing thermal resistance at the interface, there is an increase in in-plane thermal diffusion, leading to larger damage areas and deviation of Liu's interpolation model [30].

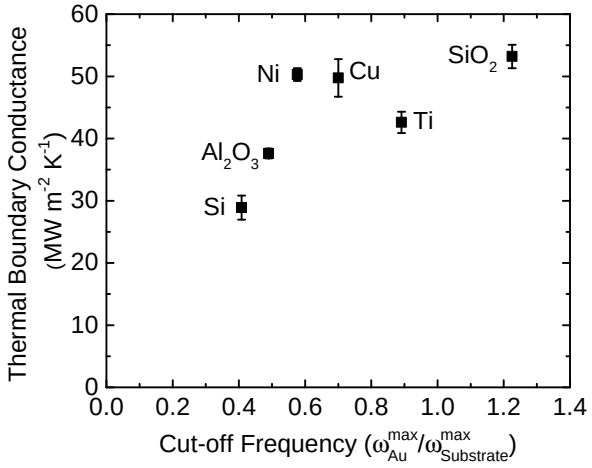

Figure 5. Thermal boundary conductance plotted as a function of the Au/substrate cutoff frequency ratios determined by phonon dispersion plots obtained in literature.

tion measurements, which is apparent in the trends in Fig. 5, which plots the thermal boundary conductance across the various Au/substrate interfaces vs. ratio of phonon cutoff frequencies between Au and the substrate ($\omega^{max}_{Au}/\omega^{max}_{Substrate}$). In general, h_K scales as the phonon spectra between the Au and substrate become better overlapped, which his consistent with several prior works [66, 67]. However, as we discuss below with regards to the mechanical coupling at the Au/substrate interface, we can not rule out changes in the bonding environment.

iii) Interfacial bonding: The influence of interfacial bonding on thermal boundary conductance has been well studied [10, 12, 24, 28, 68–71], and previous works have reported on bonding effects at Au/substrate interfaces [18, 19, 27]. In general, the thermal boundary conductance across interfaces can be influenced by both the phonon spectrum overlap (discussed above) and the interfacial bonding. Most notably, Losego et al. [27] demonstrated a direct relationship between the thermal boundary conductances across Au/self assembled monolayer/quartz interfaces and interfacial pressure determined via laser spallation experiments. This would suggest that the thermal ablation threshold in our measurements are a measure of interfacial bonding, which directly impacts the measured thermal boundary conductance.

Clearly, based on our discussion of ii and iii above, we can not distinguish between the roles of interfacial bonding and phonon spectrum overlap on the origin of the substrate dependence of thermal ablation thresholds in the thin Au films. Thus, to gain more insight into the nanoscopic mechanisms driving thermal ablation in these thin films, we conduct molecule dynamics simulations. The parameters of these simulations are discussed in detail in Section II.D. These simulations are utilized as toy models to explore the individual roles of the previously mentioned factors involved in the role of interfacial thermal transport on diffusive damage of thin films. To visualize the defected region in the computational domain after melting the region in the thin film and allowing the structure to evolve under the various ensembles, we make use of the centrosymmetry parameter, which is a measure of the local lattice disorder around an atom [72]. For an atom on an fcc lattice site, surrounded by the 12 nearest neighbor atoms on a perfect lattice, the centro-symmtry parameter will be zero, while for defects and dislocations, the centrosymmetry parameter will be high. We color the atoms based on this criteria (where the most blue atoms are described by a centro-symmetry parameter that is for a perfect lattice position and the red atoms represent a highly defected atom). Figure 6 shows the top surface of the thin film for a weakly bonded (Fig. 6a) and the strongly bonded (Fig. 6b) interfaces at 150 ps after melting. As is clear, for the weakly bonded case, the defected region is larger compared to the strongly bonded case, which is qualitatively in line with our experimental results on the measured damage area of Au films on different substrates. This suggests that the interfacial bonding (and therefore, the h_K) can influence the damaged area in thin films.

To understand the relative effect of increasing h_K on the de-

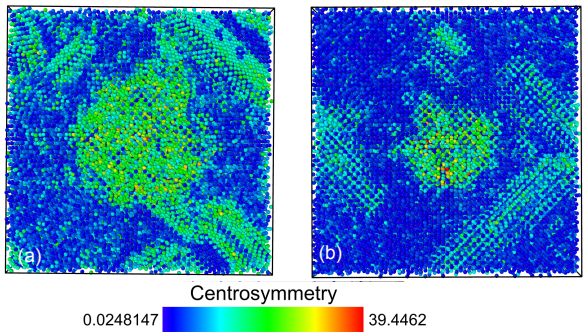

Figure 6. Top view of the computational domains with atoms colored according to their centrosymmetry parameter for the (a) weakly bonded and (b) strongly bonded interfaces.

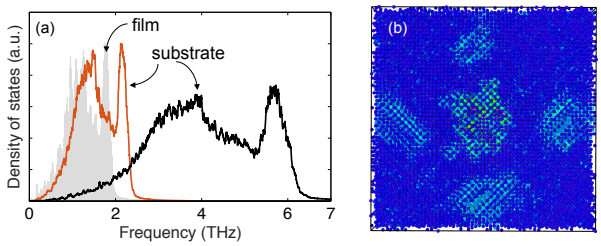

Figure 7. (a) Phonon density of states for atoms representing the thin film system and the atoms representing the substrates with 40 (black) and 280 (red) g mol^{-1}. (b) Top view of the computational domains with atoms colored according to their centrosymmetry parameter for the case where the substrate atoms have a prescribed mass of 280 g mol^{-1}. The better spectral overlap between the thin film region and the substrate atoms with a mass of 280 g mol^{-1} ensures that h_K is higher compared to the case where the substrate atoms have a lower mass.

fected area, while the interfacial bonding is set to that of the strongly bonded case, we increase the mass of the substrate atoms to 280 g mol^{-1}. This effectively shifts the spectrum of the phonon density of states (DOS) of the substrate atoms to lower frequencies and increases the overlap between the DOS of the thin film (as shown in Fig. 7a). Note, increasing the mass of the atoms from 40 g mol^{-1} to 280 g mol^{-1} reduces the thermal conductivity. However, the better spectral overlap between the thin film and the substrate region for the case where the substrate atoms have a prescribed mass of 280 g mol^{-1} ensures that h_K is increased [26]. Figure 7b shows the top view of the computational domain with the atoms colored according to their centrosymmetry parameter. The defected area for the computational domain with the better spectral overlap is greatly reduced compared to the case with the lower h_K in Fig. 6a and Fig. 6b.

V. CONCLUSION

In conclusion, the thermal ablation threshold in metal thin films is found to be dependent on the interfacial thermal resistance of the system. While our results suggest thermal confinement in the thin film is the primary ablation mechanism for picosecond laser pulses of thin films, it is likely that changes in interfacial bonding are also playing a role in the obtained threshold values. For weakly bonded systems in our simulations, the defected area surrounding the melted region is larger compared to that of a strongly bonded system, which is qualitatively in line with our experimental results on the measured damage area of Au films on different substrates. This suggests that the interfacial bonding (and therefore the h_K) can influence the damaged area in thin films. Furthermore, when the interfacial bond strength is set to that of the strongly bonded case, we increased h_K by shifting the phonon density of states (DOS) of the substrate to better overlap the DOS of the thin films. The defected area for the computational domain with better spectral overlap (and therefore larger h_K) is greatly reduced compared to the case with the lower h_K. While this model finds excellent agreement with our experimental results, where lower thermal boundary conductances ultimately lead to increased defected regions, ii and iii above can not be separated; both interfacial bonding and spectral overlap lead to similar results while the opposite term is held constant. Additionally, although typically applied for in-situ measurement of beam-waist where systems are dominated by 1-D transport, we find variation in the waist-parameter in Eq. 2 of Liu's model to provide a relative measure of transverse thermal transport for thin-film systems.

Acknowledgements

This material is based upon work supported by the Air Force Office of Scientific Research under award number FA9550-15-1-0079. D. M. Bubb and S. M. O'Malley acknowledge Awards CMMI-1531783 and CMMI-0922946 from the National Science Foundation.

* phopkins@virginia.edu

[1] E. G. Gamaly, a. V. Rode, B. Luther-Davies, and V. T. Tikhonchuk, Physics of Plasmas **9**, 949 (2002), arXiv:0102046 [physics].
[2] B. N. Chichkov, C. Momma, S. Nolte, F. von Alvensleben, and A. Tunnermann, Applied Physics A: Materials Science & Processing **63**, 109 (1996).
[3] L. V. Zhigilei, Z. Lin, and D. S. Ivanov, The Journal of Physical Chemistry C **113**, 11892 (2009).
[4] J. Yang, Y. Zhao, X. Zhu, J. Yang, Y. Zhao, and X. Zhu, Applied Physics Letters **88** (2006), 10.1063/1.2168513.
[5] P. Lorazo, L. J. Lewis, and M. Meunier, Physical Review B **73**, 1 (2006).
[6] D. von der Linde and K. Sokolowski-Tinten, Applied Surface Science **154-155**, 1 (2000).
[7] D. G. Cahill, W. K. Ford, K. E. Goodson, G. D. Mahan, A. Majumdar, H. J. Maris, R. Merlin, and S. R. Phillpot, Journal of Applied Physics **93**, 793 (2003).
[8] D. G. Cahill, P. V. Braun, G. Chen, D. R. Clarke, S. Fan, K. E. Goodson, P. Keblinski, W. P. King, G. D. Mahan, A. Majumdar, H. J. Maris, S. R. Phillpot, E. Pop, and L. Shi, Applied Physics Reviews **1** (2014), 10.1063/1.4832615.
[9] D. W. Bauerle, *Laser processing and chemistry* (Springer Science & Business Media, 2013).
[10] P. E. Hopkins, ISRN Mechanical Engineering **2013** (2013).
[11] E. T. Swartz and R. O. Pohl, Reviews of Modern Physics **61**, 605 (1989).
[12] C. Monachon, L. Weber, and C. Dames, Annual Review Of Material Research **46**, 433 (2016).
[13] P. M. Norris, N. Q. Le, and C. H. Baker, Journal of Heat Transfer **135**, 061604 (2013).
[14] P. L. Kapitza, Zhurnal Eksperimental'noi i Teoreticheskoi Fiziki **11**, 1 (1941).
[15] R. J. Stoner and J. Maris, Physical Review B **48**, 16373 (1993).
[16] J. Hohlfeld, S. Wellershoff, J. Gudde, U. Conrad, V. Jahnke, and E. Matthias, Chemical Physics **251**, 237 (2000).
[17] R. Cheaito, J. T. Gaskins, M. E. Caplan, B. F. Donovan, B. M. Foley, A. Giri, J. C. Duda, C. J. Szwejkowski, C. Constantin, H. J. Brown-Shaklee, J. F. Ihlefeld, and P. E. Hopkins, Physical Review B - Condensed Matter and Materials Physics **91**, 1 (2015).
[18] J. C. Duda, C.-Y. P. Yang, B. M. Foley, R. Cheaito, D. L. Medlin, R. E. Jones, and P. E. Hopkins, Applied Physics Letters **102**, 81902 (2013).
[19] D.-w. Oh, S. Kim, J. A. Rogers, D. G. Cahill, and S. Sinha, Advanced Materials **23**, 5028 (2011).
[20] X. Xu, Applied Surface Science **197-198**, 61 (2002).
[21] M. E. Povarnitsyn, T. E. Itina, P. R. Levashov, and K. V. Khishchenko, Physical Chemistry Chemical Physics **15**, 3108 (2013).
[22] J. Tomko, J. J. Naddeo, R. Jimenez, Y. Tan, M. Steiner, J. M. Fitz-Gerald, D. M. Bubb, and S. M. O'Malley, Physical Chemistry Chemical Physics **17**, 16327 (2015).
[23] M. E. Povarnitsyn, T. E. Itina, M. Sentis, K. V. Khishchenko, and P. R. Levashov, Physical Review B - Condensed Matter and Materials Physics **75**, 1 (2007), arXiv:0706.1371.

[24] P. E. Hopkins, M. Baraket, E. V. Barnat, T. E. Beechem, S. P. Kearney, J. C. Duda, J. T. Robinson, and S. G. Walton, Nano Letters **12**, 590 (2012).

[25] A. Giri, L. Braun, and P. E. Hopkins, Journal of Physical Chemistry C **120**, 24847 (2016).

[26] J. C. Duda, T. S. English, E. S. Piekos, W. A. Soffa, L. V. Zhigilei, and P. E. Hopkins, Physical Review B **84**, 2 (2011).

[27] M. D. Losego, M. E. Grady, N. R. Sottos, D. G. Cahill, and P. V. Braun, Nature Materials **11**, 502 (2012).

[28] R. Prasher, Applied Physics Letters **94**, 1998 (2014).

[29] J. Yang, Y. Yang, S. W. Waltermire, X. Wu, H. Zhang, T. Gutu, Y. Jiang, Y. Chen, A. A. Zinn, R. Prasher, T. T. Xu, and D. Li, Nature Nanotechnology **7**, 91 (2012).

[30] M. J. Liu, Opt. Lett. **7**, 196 (1982), arXiv:arXiv:1011.1669v3.

[31] M. Amin, J. Tomko, J. Naddeo, R. Jimenez, D. Bubb, M. Steiner, J. Fitz-Gerald, and S. O'Malley, Applied Surface Science **348**, 30 (2015).

[32] N. Sanner, O. Utéza, B. Bussiere, G. Coustillier, a. Leray, T. Itina, and M. Sentis, Applied Physics A: Materials Science and Processing **94**, 889 (2009).

[33] P. E. Hopkins, J. C. Duda, B. Kaehr, X. W. Zhou, C. Y. Peter Yang, and R. E. Jones, Applied Physics Letters **103**, 0 (2013).

[34] P. E. Hopkins, L. M. Phinney, S. P. Kearney, T. W. Grasser, and C. T. Harris, International Journal of Heat and Mass Transfer **132**, 1 (2010).

[35] A. Giri, J. T. Gaskins, B. F. Donovan, C. Szwejkowski, R. J. Warzoha, M. A. Rodriguez, J. Ihlefeld, and P. E. Hopkins, Journal of Applied Physics **117** (2015), 10.1063/1.4914867.

[36] P. M. Norris, A. P. Caffrey, R. J. Stevens, M. J. Klopf, J. T. McLeskey Jr., and A. N. Smith, Review of Scientific Instruments **74** (2003), 10.1063/1.1517187.

[37] B. M. Clemens, G. L. Eesley, and C. A. Paddock, Physical Review B **37** (1988).

[38] R. M. Costescu, M. A. Wall, and D. G. Cahill, Physical Review B **67**, 1 (2003).

[39] D. G. Cahill, Review of Scientific Instruments **75**, 5119 (2004).

[40] A. J. Schmidt, X. Chen, and G. Chen, Review of Scientific Instruments **79** (2008), 10.1063/1.3006335.

[41] D. R. Lide, *CRC Handbook of Chemistry and Physics, 74th Edition* (1994).

[42] E. R. Dobrovinskaya, L. A. Lytvynov, and V. Pishchik, *Sapphire: Material, Manufacturing, Applications* (Springer, 2009).

[43] D. D. L. Chung, Applied Thermal Engineering **21**, 1593 (2001).

[44] W. G. Hoover, Physical Review A **31**, 1695 (1985).

[45] A. J. H. Mcgaughey and M. Kaviany, International Journal of Heat and Mass Transfer **47**, 1783 (2004).

[46] M. S. Brown and C. B. Arnold, in *Springer Series in Materials Science*, Springer Series in Materials Science, Vol. 135, edited by K. Sugioka, M. Meunier, and A. Piqué (Springer Berlin Heidelberg, Berlin, Heidelberg, 2010) Chap. 4, pp. 91–120.

[47] D. Wortmann, J. Koch, M. Reininghaus, C. Unger, C. Hulverscheidt, D. Ivanov, and B. N. Chichkov, Journal of Laser Applications **24** (2012), 10.2351/1.4734048.

[48] P. Delaporte and A.-P. Alloncle, Optics & Laser Technology **78**, 33 (2016).

[49] M. Domke, L. Nobile, S. Rapp, S. Eiselen, J. Sotrop, H. P. Huber, and M. Schmidt, Physics Procedia **56**, 1007 (2014).

[50] M. E. Povarnitsyn and T. E. Itina, Applied Physics A: Materials Science and Processing **117**, 175 (2014).

[51] C. Shih, M. V. Shugaev, C. Wu, and L. V. Zhigilei, Journal of Physical Chemistry C **Just Accep** (2017).

[52] Z. Ge, D. G. Cahill, and P. V. Braun, Physical Review Letters **96**, 1 (2006), arXiv:arXiv:1402.6991v1.

[53] M. E. Caplan, A. Giri, and P. E. Hopkins, Journal of Chemical Physics **140** (2014), 10.1063/1.4870778.

[54] B. Rethfeld, K. Sokolowski-Tinten, D. von der Linde, and S. I. Anisimov, Applied Physics A **769**, 767 (2004).

[55] P. E. Hopkins, J. C. Duda, and P. M. Norris, Journal of Heat Transfer **133**, 1 (2011).

[56] P. E. Hopkins and P. M. Norris, Journal of Heat Transfer **131**, 1 (2009).

[57] P. E. Hopkins, Journal of Applied Physics **108** (2009), 10.1063/1.3169515.

[58] P. E. Hopkins, P. M. Norris, and R. J. Stevens, Journal of Heat Transfer **130** (2008), 10.1115/1.2787025.

[59] H.-k. Lyeo and D. G. Cahill, Physical Review B **73**, 1 (2006).

[60] A. Giri, P. E. Hopkins, J. G. Wessel, J. C. Duda, A. Giri, P. E. Hopkins, J. G. Wessel, and J. C. Duda, Journal of Applied Physics **118** (2016), 10.1063/1.4934511.

[61] P. E. Hopkins, J. L. Kassebaum, and P. M. Norris, Journal of Applied Physics **105** (2009), 10.1063/1.3068476.

[62] P. E. Hopkins and P. M. Norris, Applied Surface Science **253**, 6289 (2007).

[63] A. Giri, B. M. Foley, and P. E. Hopkins, Journal of Heat Transfer **136**, 1 (2014).

[64] G. T. Hohensee, R. Wilson, and D. G. Cahill, Nature Communications **6**, 1 (2015).

[65] J. C. Duda, T. E. Beechem, J. L. Smoyer, P. M. Norris, and P. E. Hopkins, Journal of Applied Physics **108** (2010), 10.1063/1.3483943.

[66] R. J. Stevens, A. N. Smith, and P. M. Norris, Journal of Heat Transfer **127**, 315 (2005).

[67] P. M. Norris and P. E. Hopkins, Journal of Heat Transfer **131**, 043207 (2009).

[68] M. Shen, W. J. Evans, D. Cahill, and P. Keblinski, Physical Review B **84**, 1 (2011).

[69] P. J. O'Brien, S. Shenogin, J. Liu, P. K. Chow, D. Laurencin, P. H. Mutin, M. Yamaguchi, P. Keblinski, and G. Ramanath, Nature Materials **12**, 118 (2012).

[70] B. M. Foley, S. C. Herna, J. C. Duda, J. T. Robinson, S. G. Walton, and P. E. Hopkins, Nano Letters **15**, 4876 (2015).

[71] C. Monachon, G. Schusteritsch, E. Kaxiras, L. Weber, C. Monachon, G. Schusteritsch, E. Kaxiras, and L. Weber, Journal of Applied Physics **115** (2014), 10.1063/1.4869668.

[72] C. L. Kelchner, S. J. Plimpton, and J. C. Hamilton, Physical Review B **58**, 85 (1998).